Low-Band-Gap Platinum Acetylide Polymers as Active Materials for Organic Solar Cells

Jianguo Mei,[†,‡] Katsu Ogawa,[†,‡] Young-Gi Kim,[†,‡] Nathan C. Heston,[†,‡] Daniel J. Arenas,[‡,§] Zahra Nasrollahi,[‡,§] Tracy D. McCarley,[∥] David B. Tanner,[‡,§] John R. Reynolds,*[,†,‡] and Kirk S. Schanze*[,†,‡]

Departments of Chemistry and Physics and Center for Macromolecular Science and Engineering, University of Florida, Gainesville, Florida 32611-7200, and Department of Chemistry, Louisiana State University, Baton Rouge, Louisiana 70803-1804

ABSTRACT We report on two pairs of platinum acetylide based polymers and model oligomers utilizing a 2,1,3-benzothiadiazole (BTD) acceptor moiety flanked on either side by either 2,5-thienyl donor units (Pt_2BTD-Th and p-PtBTD-Th) or (3,4-ethylenedioxy)-2,5-thienyl donors (Pt_2BTD-EDOT and p-PtBTD-EDOT). Both oligomer/polymer pairs absorb strongly throughout the visible region; however, because the (ethylenedioxy)thiophene moiety is a stronger donor than thiophene, the latter oligomer/polymer pair has a correspondingly lower band gap and, therefore, harvests light more efficiently at longer wavelengths. p-PtBTD-Th exhibits a relatively narrow molecular weight distribution with a number-average molecular weight (M_n) of 22 kDa, while p-PtBTD-EDOT exhibits a comparable M_n of 33 kDa but has a high polydispersity index likely due to aggregation. We provide a complete report of the photophysical and electrochemical characterization of the two oligomer/polymer pairs. The photophysical studies reveal that the materials undergo relatively efficient intersystem crossing. In a discussion of the energetics of photoinduced electron transfer from the platinum polymers to [6,6]-phenyl C_{61} butyric acid methyl ester (PCBM), it is noted that while the singlet state is quenched efficiently, the triplet state is not quenched, indicating that charge generation in the photovoltaic materials must ensue from the singlet manifold. Finally, organic photovoltaic devices based on blends of p-PtBDT-Th or p-PtBDT-EDOT with PCBM were characterized under monochromatic and simulated solar (AM1.5) illumination. Optimized devices exhibit an open-circuit voltage (V_{oc}) of ~0.5 V, a short-circuit current density (I_{sc}) of ~7.2 mA cm^{-2}, and a fill factor of ~35%, which yields overall power conversion efficiencies of 1.1−1.4%.

KEYWORDS: solar cell • organometallic polymer • conjugated polymer • triplet state • fullerene

INTRODUCTION

Conjugated polymers (CPs) and oligomers have drawn significant attention as the active materials for organic photovoltaic devices (OPVs) because of their potential to enable the development of plastic solar cells that are lightweight, flexible, and low cost (1−3). Since the discovery of rapid photoinduced electron transfer (PET) from poly[2-methoxy-5-(2′-ethylhexyloxy)-*p*-phenylenevinylene] to C60 (4, 5), the use of fullerene derivatives as the electron acceptor in OPVs has become prevalent. The most common approach to the fabrication of CP-based OPV active materials is to prepare a blend of a CP and a fullerene derivative such as [6,6]-phenyl-C_{61}-butyric acid methyl ester (PCBM) to produce a bulk heterojunction. The current state-of-the-art single-layer CP-based OPVs achieve power conversion efficiency in the range of 5−5.5%, while the highest reported efficiency of 6.5% is for a tandem solar cell (6−13). Solar cells with optimized performance have been developed using poly(3-hexylthiophene)/PCBM blends (14), and these cells feature nearly ideal photon-to-current quantum efficiency (IPCE) in the mid-visible region. However, the barrier that must be overcome to produce highly efficient OPVs is to extend the light absorption into the near-infrared region and at the same time preserve the high IPCE and open-circuit voltage. At a fundamental level, the efficiency of several factors is key to the overall efficiency of the device: light-harvesting efficiency across the visible and near-infrared regions, exciton diffusion to the donor−acceptor interface, photoinduced charge separation, and mobility of the charge carriers produced by photoinduced charge separation (1).

We have an interest in exploring whether triplet excited states can be harnessed to increase the efficiency of charge generation in OPV active materials (15, 16). At a fundamental level, there are several reasons why the triplet state might be expected to give rise to efficient charge generation. First, the long lifetime of the triplet state may enhance the probability of exciton diffusion to a donor−acceptor interface (17, 18). Second, quantum mechanical spin restrictions prevent charge recombination in the geminate ion-radical pair produced as a result of photoinduced charge transfer from a triplet-state precursor (19). Triplet states are not produced efficiently as a result of direct excitation of most organic conjugated materials. Therefore, in order to explore the effects of triplet states on OPVs, it is necessary to utilize materials that incorporate heavy atoms, which give rise to efficient intersystem crossing by enhancing the spin−orbit coupling (20).

* To whom correspondence should be addressed. E-mail: kschanze@chem.ufl.edu (K.S.S.), reynolds@chem.ufl.edu (J.R.R.).
Received for review October 7, 2008 and accepted November 29, 2008
† Department of Chemistry, University of Florida.
‡ Center for Macromolecular Science and Engineering, University of Florida.
§ Department of Physics, University of Florida.
∥ Louisiana State University.
DOI: 10.1021/am800104k

Published on Web 01/13/2009

Scheme 1. Structures of Platinum Acetylide Model Compounds and Polymers

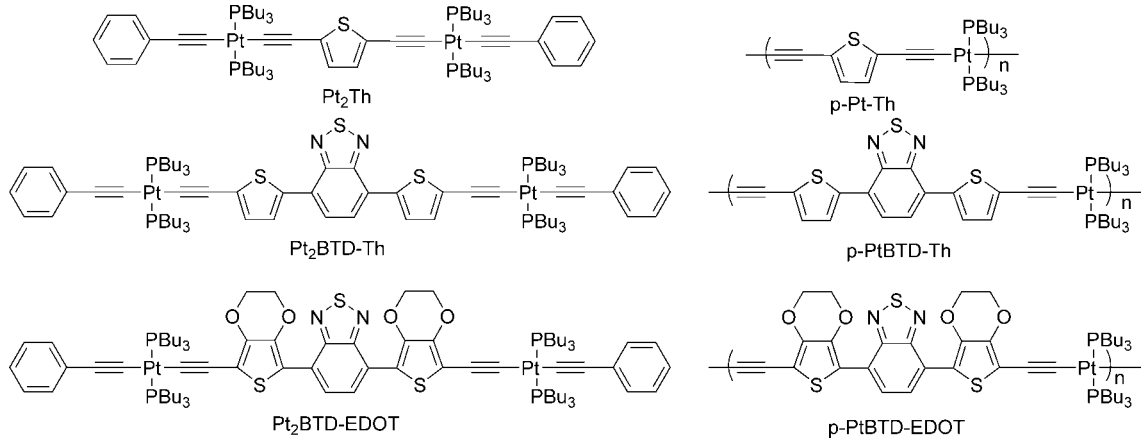

Platinum acetylide oligomers and polymers have been studied widely because they represent a class of π-conjugated materials featuring high quantum efficiency for intersystem crossing (to produce the triplet excited state) following direct excitation, providing considerable insight concerning the electronic structure, delocalization, and dynamics of the triplet exciton (21−26). Platinum acetylides have also been used as the active materials in organometallic photovoltaic devices. An early example by Köhler and co-workers demonstrated that the photocurrent response of a blend of a platinum acetylide polymer and C_{60} was enhanced relative to the pure polymer (27). Evidence that the polymer triplet state was active in charge generation came from the observation that C_{60} only partially quenched the polymer's singlet emission (fluorescence) but completely quenched the triplet emission (phosphorescence). More recently, we reported a photophysical and OPV device study that focused on active materials consisting of blends of the platinum acetylide polymer *p*-PtTh (Scheme 1) and PCBM (15, 16). Luminescence quenching and transient absorption spectroscopy indicate that PET from the *p*-PtTh triplet to PCBM is efficient. Solar cells constructed using a 4:1 PCBM/*p*-PtTh blend as the active material exhibit a peak IPCE of *ca.* 10% and an overall power conversion efficiency of 0.27%. While the IPCE of the *p*-PtTh/PCBM cells is respectable, the overall power conversion efficiency is limited because *p*-PtTh only absorbs blue light ($\lambda_{max} \approx 411$ nm), and consequently its absorption overlaps poorly with the solar spectrum.

In a natural continuation of our investigation of the triplet excited state in OPVs, we sought to develop platinum acetylide polymers that absorb light strongly throughout the visible region. It was believed that such materials would lead to more efficient photocurrent generation because of increased light-harvesting efficiency while preserving the high intersystem yields afforded by the presence of the platinum heavy metal centers in the π-conjugated chain. In order to achieve this objective, we designed a series of polymers and model oligomers that feature π-conjugated segments of the type donor−acceptor−donor alternating with (or end-capped by) *trans*-Pt$(PBu_3)_2$ units (Scheme 1). These materials were developed on the basis of prior work demonstrating that low-band-gap polymers and oligomers can be prepared when the conjugated backbone consists of alternating repeat units that have donor and acceptor properties (28−36). Two pairs of polymers and model oligomers are the focus of the work presented herein. The first pair features a π-conjugated segment consisting of a 2,1,3-benzothiadiazole (BTD) acceptor moiety flanked on either side by 2,5-thienyl donor units (Pt_2BTD-Th and *p*-PtBTD-Th; Scheme 1), whereas in the second pair, the BTD unit is flanked by (3,4-ethylenedioxy)-2,5-thienyl donors (Pt_2BTD-EDOT and *p*-PtBTD-EDOT; Scheme 1). Both oligomer/polymer pairs absorb strongly throughout the visible region; however, because the (ethylenedioxy)thiophene moiety is a stronger donor than thiophene, the latter oligomer/polymer pair has a correspondingly lower band gap and, therefore, harvests light more efficiently in the near-infrared region.

Here, we provide a complete report of the syntheses and photophysical and electrochemical characterization of the two oligomer/polymer pairs. In addition, we have characterized the ability of the materials to undergo PET to PCBM from both the singlet and triplet excited-state manifolds. Finally, OPVs based on blends of *p*-PtBTD-Th or *p*-PtBTD-EDOT with PCBM were characterized under monochromatic and simulated solar (AM1.5) illumination. The photophysical studies reveal that the materials undergo relatively efficient intersystem crossing. However, while the singlet state is quenched efficiently by PCBM, the triplet state is not quenched, indicating that charge generation in the photovoltaic materials must ensue from the singlet manifold. A thermodynamic analysis of PET based on the electrochemical and spectroscopic data indicates that charge transfer from the singlet state of the low-band-gap platinum acetylides is thermodynamically feasible but not from the triplet state. Nevertheless, the materials perform well when used as bulk heterojunctions in OPV devices. Operating under AM1.5 conditions, optimized devices exhibit an open-circuit voltage (V_{oc}) of ~0.5 V, a short-circuit current density (I_{sc}) of ~7.2 mA cm^{-2}, and a fill factor of ~35%, which yields overall power conversion efficiencies of 1.1−1.4%.

While this paper was under preparation, a report by Wong and co-workers appeared describing the fabrication and characterization of OPVs fabricated with blends of PCBM and *p*-PtBTD-Th, which is one of the two platinum acetylide

polymers that is the focus of the work herein (37, 38). The OPVs tested by Wong's group are believed to operate with remarkably high efficiency; a peak IPCE of 87% at around 575 nm is reported, and the overall efficiency of a cell operating under AM1.5 illumination was reported to be 4.93% (37). It should be noted that the technical accuracy of these reported values has been examined by others, and a careful analysis of the results is required for these photovoltaic cells (39, 40). The complete study reported herein provides an interesting and useful complement and contrast to the materials-oriented study by the Wong group because we have fully characterized the photophysics, electrochemistry, and photoredox properties of two structurally related low-band-gap platinum acetylide polymers as well as characterized their performance in bulk heterojunction OPV devices. An important point is that the devices characterized in our hands operate with lower efficiency compared to those in the previous report (37). Possible origins for this discrepancy in device performance are considered in our discussion.

EXPERIMENTAL SECTION

General Synthetic Procedures and Source of Starting Materials. All chemicals used for synthesis were of reagent grade and purchased from Sigma-Aldrich Chemical Co. unless otherwise noted. The poly[(3,4-ethylenedioxy)thiophene]/poly-(styrenesulfonate) (PEDOT-PSS) used was Baytron P VP Al 4083. PCBM was purchased from SES Research, Houston, TX. All procedures involving air- and moisture-sensitive reagents were performed using standard Schlenk techniques. Toluene was purified with a dry solvent system. The procedures for the preparation of compounds **1** and **2** are described in the Supporting Information. 1,2-Dichlorobenzene (ODCB) was distilled from calcium hydride under a nitrogen atmosphere.

***p*-PtBTD-Th.** Compound **1** (0.20 mmol, 69.6 mg), *trans*-$Pt(PBu_3)_2Cl_2$ (0.20 mmol, 134.1 mg), and CuI (1.0 mg) were added to a Schlenk flask. After three cycles of vacuum and argon, piperidine/toluene [1:1 (v/v), 8 mL] was injected through a septum. The mixture was stirred at room temperature for 24 h and then passed through a bed of neutral alumina to remove catalysts. The solvent was removed under reduced pressure. The dark-purple solid (film) was redissolved into a minimum amount of $CHCl_3$ and the solution poured into cold methanol. The precipitation was repeated three times. A fibrous purple product (144 mg, 73%) was obtained after final filtration. Further purification was effected through Soxhlet extraction by methanol, hexane, and $CHCl_3$. ^{1}H NMR (300 MHz, C_6D_6): δ 8.11 (d, J = 4 Hz, 2H), 7.40 (s, 2H), 7.27 (d, J = 4 Hz, 2H), 2.20−2.24 (m, 12H), 1.74−1.77 (m, 12H), 1.47−1.59 (m, 12H), 1.03 (t, J = 7.5 Hz, 18H). ^{31}P NMR (121 MHz, C_6D_6): δ 5.11 (J_{Pt-P} = 2336 Hz). GPC: M_n = 22 000 g/mol, PDI = 1.9. FT-IR (KBr): 2955, 2871, 2884, 2084, 1481, 1440, 801, 667 cm^{-1}.

***Pt*$_2$BTD-Th.** To a 100 mL Schlenk flask were added compound **1** (0.1 mmol, 34.8 mg) and *trans*-ethynylphenylchlorobis(tri-*n*-butylphosphine)platinum(II) (0.2 mmol, 147.3 mg). After three cycles of vacuum and argon, degassed piperidine/toluene [1:1 (v/v), 10 mL] was injected through a septum. The resulting mixture was stirred under mild reflux overnight. Upon cooling to room temperature, silica gel was added to the purple solution, and the solvent was evaporated. The product was purified by column chromatography using ethyl acetate/hexane (5:95) as the eluent. The desired product Pt_2BTD-Th was obtained in 87% yield after drying (143.9 mg). ^{1}H NMR (300 MHz, C_6D_6): δ 8.09 (d, J = 4 Hz, 2H), 7.63 (d, J = 8 Hz, 4H), 7.37 (s, 2H), 7.24 (d, J = 4 Hz, 2H), 7.17 (m, 4H), 7.01 (t, J = 7.5 Hz, 2H), 2.12−2.19 (m, 24H), 1.64−1.77 (m, 24H), 1.39−1.51 (m, 24H), 0.94 (t, J = 7.5 Hz, 18H). ^{13}C NMR (75 MHz, C_6D_6): δ 152.9, 136.7, 132.2, 131.1, 129.9, 128.5, 128.4, 125.7, 125.3, 124.8, 119.0 (t), 110.1, 108.2 (t), 102.5, 26.9 (m) 24.8 (m), 24.5, 14.0 (due to superimposition, one carbon is missing). ^{31}P NMR (121 MHz, C_6D_6): δ 4.93 (J_{Pt-P} = 2356 Hz). HRMS (MALDI-TOF, terthiophene as the matrix). Calcd for $C_{82}H_{122}N_2P_4S_3Pt_2$: *m*/*z* 1744.7010. Found: *m*/*z* 1744.7170.

***p*-PtBTD-EDOT.** Compound **2** (0.2 mmol, 122 mg) and *trans*-$Pt(PBu_3)_2Cl_2$ (0.2 mmol, 134 mg) were added to a Schlenk flask charged with a stir bar. After degassing, piperidine/toluene [1:2 (v:v), 15 mL] was injected through a septum at 0 °C followed by a solution of tetrabutylammonium fluoride (TBAF; 0.5 mmol, 1 M in tetrahydrofuran, THF). The color of the resulting solution turned from red to blue, and the mixture was stirred for 24 h at room temperature. After removal of the solvent under reduced pressure, the blue solid (film) was dissolved into $CHCl_3$ and passed through a bed of alumina. The filtrate was concentrated and precipitated from methanol. A blue solid was obtained (177 mg, 83%). Further purification was effected through Soxhlet extraction by methanol, hexane, and $CHCl_3$. ^{1}H NMR (300 MHz, C_6D_6): δ 8.68 (s, 2H), 3.57−3.52 (m, 8H), 2.34−2.30 (m, 12H), 1.81−1.78 (m, 12H), 1.64−1.54 (m, 12H), 1.00 (t, J = 7.2 Hz, 18H). ^{31}P NMR (121 MHz, C_6D_6): δ 4.20 (J = 2365 Hz). GPC: M_n = 33 000 g/mol, PDI = 16.

***Pt*$_2$BTD-EDOT.** To a 100 mL Schlenk flask were added compound **2** (0.05 mmol, 30.5 mg) and *trans*-ethynylphenylchlorobis(tri-*n*-butylphosphine)platinum(II) (0.1 mmol, 73.6 mg) and CuI (19 mg). After degassing, piperidine/toluene [1:1 (v/v), 10 mL] was injected through a septum. Upon the addition of TBAF (0.2 mL, 1 M in THF), the solution turned from red to purple-blue and the resulting mixture was stirred under ambient temperature overnight. The solvent was evaporated under reduced pressure. The product was purified by chromatography using hexane/ethyl acetate (3:1) as the eluent. The desired product Pt_2BTD-EDOT was obtained in 74% yield (69.5 mg). ^{1}H NMR (300 MHz, C_6D_6): δ 8.67 (s, 2H), 7.63 (d, J = 7.6 Hz, 4H), 7.19 (m, 4H), 7.17 (t, J = 7.0 Hz, 2H), 3.51−3.48 (m, 8H), 2.23−2.15 (m, 24H), 1.70−1.64 (m, 24H), 1.54−1.42 (m, 24H), 0.95 (t, J = 1 Hz, 36H). ^{13}C NMR (75 MHz, C_6D_6): δ 153.0, 141.4, 140.5, 131.2, 130.1, 126.1, 125.2, 124.0, 121.2 (t, J = 14.7 Hz), 111.5, 110.4, 109.1, 109.1, 108.9 (t, J = 14.7 Hz), 99.8 (t, J = 1.8 Hz), 64.6, 64.0, 26.9 (m) 24.7 (m), 24.5 (m), 14.1. ^{31}P NMR (121 MHz, C_6D_6): δ 4.48 (J_{Pt-P} = 2360 Hz). HRMS (MALDI-TOF, terthiophene as the matrix). Calcd for $C_{86}H_{128}N_2O_4P_4S_3Pt_2$ (M^+): *m*/*z* 1863.7292. Found: *m*/*z* 1863.7432.

Characterization Methods. Unless otherwise noted, ^{1}H, ^{13}C, and ^{31}P NMR spectra were recorded on either a Varian Gemini 300 or a Mercury 300 spectrometer, and chemical shifts are reported in ppm relative to tetramethylsilane. Mass spectra were recorded on either a Finnigan MAT95Q Hybrid Sector (EI, HRMS) or a Bruker Reflex II (MALDI-TOF) mass spectrometer or Bruker Proflex III (MALDI-TOF) operated in linear mode with delayed extraction. The cyclic voltammetry (CV) experiments were performed on a Bioanalytical Systems CV50W electrochemical analyzer at a sweep rate of 100 mV/s using a platinum disk working electrode, a carbon disk auxiliary electrode, and a Ag/Ag^+ reference electrode. Solutions of samples were prepared in dichloromethane with 0.10 M tetrabutylammonium hexafluorophosphate ($TBAPF_6$) as the supporting electrolyte. At the end of each measurement, ferrocene (Fc) was added to the mixture as an internal standard for the potential. All potentials are reported with respect to the potential of a Fc/Fc^+ redox couple (−4.8 eV vs vacuum).

Photophysical Measurements. Steady-state UV−visible absorption spectra were obtained on a Perkin-Elmer Lambda 25 dual-beam absorption spectrometer using 1 cm quartz cells. Steady-state fluorescence emission spectra were recorded on a SPEX TRIAX 180 spectrograph coupled with a Spectrum One

CCD detector. Steady-state near-infrared fluorescence spectra were recorded on a SPEX-2 fluorescence spectrophotometer with an indium−gallium−arsenide (InGaAs) detector. Fluorescence decays were obtained by time-correlated single photon counting on an instrument that was constructed in-house. A violet diode laser (405 nm; IBH instruments, Edinburgh, Scotland; pulse width 800 ps) was used as the excitation source. Transient absorption difference spectra were collected using a 2-mm-path-length cell on an apparatus described elsewhere (41). Solutions were prepared in ODCB and purged with argon for 30 min before each measurement. The third harmonic (355 nm) of a Continuum Surelite II-10 Nd:YAG laser was augmented with a Continuum Surelite OPO Plus optical parametric oscillator to provide 550 nm laser pulses (10 mJ pulse^{-1}) as the excitation source.

Photovoltaic Device Fabrication and Characterization. Solar cells were fabricated on indium−tin oxide (ITO)-covered glass substrates (Delta Technologies; $R_s = 8-12\ \Omega$/square). The ITO/glass substrates were etched by exposure to aqua regia vapor and subsequently cleaned in an ultrasonic bath for 15 min with aqueous sodium dodecyl sulfate (Fisher Scientific), deionized water (Milli-Q), acetone, and isopropyl alcohol. The substrates were then treated with oxygen plasma for 15 min in a Plasma Cleaner (Harrick PDC-32G). An aqueous PEDOT-PSS solution (Baytron P VP Al 4083) was spin-coated at 4000 rpm onto the cleaned glass substrates, and the resulting polymer film was dried under vacuum for 10 min at 150 °C. A solution of the photoactive material (*p*-PtBTD-Th or *p*-PtBTD-EDOT and PCBM, 1:4 weight ratio of polymer/PCBM) was prepared in toluene or *o*-dichlorobenzene with solids added at 1−2% by weight. The solution of the photoactive materials was then spin-coated onto the PEDOT-PSS-coated substrate in an inert-atmosphere box (M-Braun) under argon, and the resulting films were dried under high vacuum overnight at room temperature. The thickness of the active layer was measured using a Dektak 3030 (Veeco Instruments Inc.) profilometer. (Each thickness reported in this study is the average of at least three different measurements on different regions of the film.) Aluminum (100 nm) was deposited by thermal evaporation on the photoactive layer. The active area of the devices was 0.25 cm^2. Note that the entire process of active layer spin coating and electrode evaporation was carried out inside of the inert-atmosphere glovebox.

The current−voltage (*I*−*V*) characteristics were measured with a Keithley SMU 2400 source measurement unit under an illumination of AM1.5 with an incident power density of 100 mW cm^{-2} using a 150 W xenon arc lamp power supply (Oriel Instruments). The external quantum efficiency of the photovoltaic devices was evaluated by measuring the IPCE (%). For IPCE measurements, device pixels were irradiated with monochromatic light through an ISA H20 monochromator with a 75 W xenon arc lamp as the light source. The intensity of the source at each wavelength was determined using an energy meter (S350, UDT Instruments) equipped with a calibrated silicon detector (model 221, UDT Instruments). The current response under short-circuit conditions was then recorded for each pixel at 10 nm intervals using a Keithley 2400 SMU (positive lead to ITO and negative lead to aluminum). The current−voltage (*I*−*V*) curve and IPCE plots were measured for at least three pixels, and the data represent the average of the three measurements. The measurements were performed in air without encapsulation.

RESULTS

Polymer Synthesis and Characterization. The general synthetic routes used to prepare the two oligomer/polymer pairs are illustrated in Scheme 2. Detailed syntheses and characterization data for the starting compounds (**1**−**3**) are provided in the Supporting Information. Compound **1** was reacted with *trans*-Pt(PBu$_3$)$_2$Cl$_2$ in the presence of a catalytic amount of CuI and piperidine in toluene to afford the polymer *p*-PtBTD-Th as a material soluble in THF, chloroform, and toluene. The phenylethynyl end-capped model oligomer Pt$_2$BTD-Th was obtained in good yield by reacting **1** with **3** in the presence of CuI. A similar strategy was used to prepare *p*-PtBTD-EDOT and Pt$_2$BTD-EDOT with a slight modification in the procedure. Specifically, because of the fact that removal of the trimethylsilyl protecting groups by reaction of **2** with TBAF led to decomposition of the product, a methodology was adopted whereby **2** was deprotected in situ. Thus, reaction of **2** with TBAF in the presence of either *trans*-Pt(PBu$_3$)$_2$Cl$_2$ or **3** afforded the expected products, *p*-PtBTD-EDOT or Pt$_2$BTD-EDOT, respectively.

Scheme 2. General Synthetic Scheme of Model Compounds and Polymers

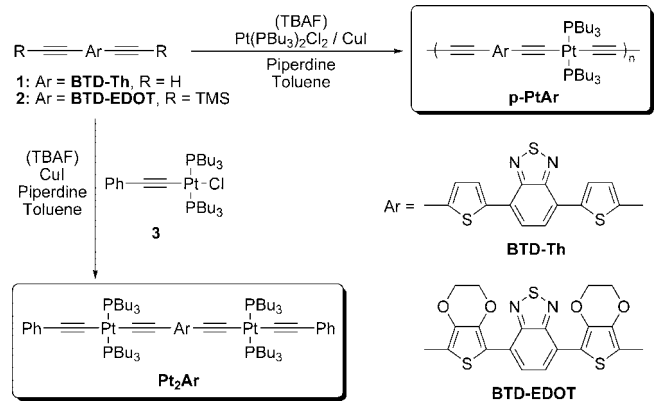

The oligomers Pt$_2$BTD-Th and Pt$_2$BTD-EDOT were purified by silica gel column chromatography, and the ^{1}H, ^{13}C, and ^{31}P NMR spectra of the isolated products are consistent with their molecular structures. The polymer samples were purified by precipitation from a $CHCl_3$ solution into methanol and then subjected to Soxhlet extraction by methanol, hexane, and $CHCl_3$ for further purification. The ^{1}H and ^{31}P NMR spectra of the polymers are in good agreement with the structure of the materials (NMR spectra for the oligomers and polymers are provided in the Supporting Information).

Gel permeation chromatography (GPC) was performed on polymer samples using chloroform as the eluent, and molecular weights are referenced to polystyrene standards. The GPC chromatogram of *p*-PtBTD-Th exhibits a relatively narrow molecular weight distribution with a number-average molecular weight (M_n) of 22 kDa and a polydispersity index (PDI) of 1.97. By contrast, while *p*-PtBTD-EDOT exhibits a comparable M_n of 33 kDa, the PDI of the polymer is unreasonably high. The broad polydispersity observed for *p*-PtBTD-EDOT is likely due to the fact that this polymer has a lower solubility and, consequently, it tends to aggregate. This premise is supported by the observation that the GPC polydispersity of *p*-PtBTD-EDOT varies with the concentration of the solution used for the analysis.

Matrix-assisted laser desorption−ionization (MALDI) mass spectroscopy was carried out on samples *p*-PtBTD-Th and *p*-PtBTD-EDOT in an effort to obtain additional information concerning the molecular weight distribution of the poly-

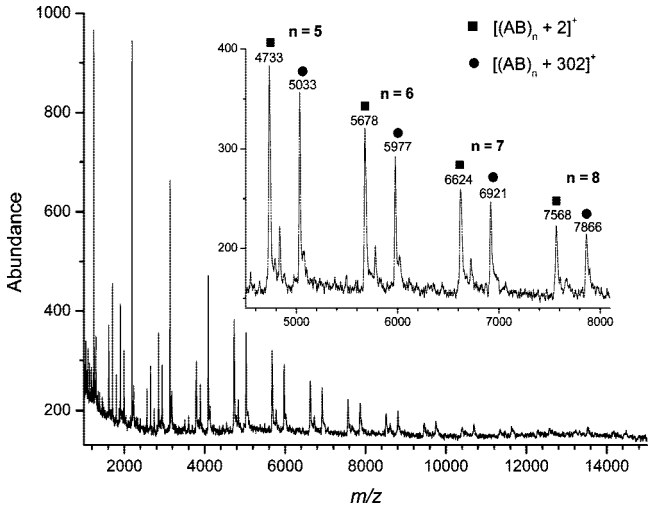

FIGURE 1. MALDI-TOF mass spectrum of *p*-PtBTD-Th.

mers, as shown in Figures 1 and S2 in the Supporting Information. MALDI was performed using 2-[(2E)-3-(4-*tert*-butylphenyl)-2-methylprop-2-enylidene]malonitrile as a matrix (42). The *p*-PtBTD-Th MALDI mass spectrum exhibits peaks spanning from *m/z* 1000 to 15 000 with several ion series observed in the spectrum. Ions in each series are separated by 946 amu, which is consistent with the repeat unit structure of the polymer (see Scheme 1). Above *m/z* 4100, there are two main series. The most intense is $[(AB)_n + 2]^+$. It is suspected that the residual mass of 2 amu could represent two hydrogen end groups. However, at this mass the accuracy of the instrument is insufficient to distinguish between linear compounds with two hydrogen end groups and cyclic compounds. $[(AB)_n + 302]^+$ is the other main series at higher masses. In contrast, the *p*-PtBTD-EDOT MALDI mass spectrum has ion series spanning only from *m/z* 1000 to 9000. This may result from high mass discrimination on the part of the instrument or polymer with low molecular weight. Ions in each series are separated by 1062 amu, consistent with the repeat unit structure of this polymer. Below *m/z* 5000, there are related series of $[(AB)_n + 672]^+$, $[(AB)_n + 764]^+$, and $[(AB)_n + 855]^+$. These series correspond to $B(AB)_n$ polymers with two chlorine end groups, one chlorine and one iodine end group, and two iodine end groups, respectively ($n = 1-5$). Above *m/z* 5000, the predominant series is $(AB)_n^+$ with $n = 5-8$. Interestingly, end groups of two chlorines, one chlorine/one iodine, and two iodines, similar to the end groups in the lower mass series, do not exist (note that the iodine content can be contributed from the CuI catalyst).

Differential scanning calorimetry and thermal gravimetric analysis (DSC and TGA) were carried out on the polymers to seek information regarding their thermal properties and thermal stability. The DSC data indicated that both polymers lack any specific thermal transitions over the temperature range −100 to +250 °C. The TGA results indicate that the decomposition temperatures are 300 and 325 °C for *p*-PtBTD-Th and *p*-PtBTD-EDOT, respectively.

Electrochemistry. CV and differential pulse voltammetry (DPV) were performed in order to characterize the accessible redox states of the compounds and to obtain the oxidation and reduction potentials for the redox processes. When combined with the photophysical data (vide infra), the electrochemical potentials can be used to estimate the driving force for PET from the polymers to PCBM as an acceptor. A summary of the electrochemical data is provided in Table 1 and representative cyclic voltammograms of Pt_2BTD-Th and *p*-PtBTD-Th are shown in Figure 2. The cyclic voltammograms of Pt_2BTD-EDOT and *p*-PtBTD-EDOT are shown in Figure S3 in the Supporting Information. Perusal of the tabular listing and figure reveals that all of the materials exhibit a single, reversible reduction at negative potentials and two oxidation waves at positive potentials. As outlined below, all of the waves can be attributed to oxidation/reduction of electrophores concentrated on the π-conjugated segments that contain the three heterocyclic rings [Th-BTD-Th and EDOT-BTD-EDOT, where Th = thienyl, BTD = benzo[1,2,5]thiadiazole, and EDOT = (3,4-ethylenedioxy)thiophene]. In particular, the reduction waves occur at ca. $E_{1/2} = -1.75$ V (−1.85 V for the EDOT series), which corresponds closely to the reduction potentials previously reported for the "free oligomers", i.e., Th-BTD-Th and EDOT-

Table 1. Electrochemical Properties of Model Compounds and Polymers[a]

	$E_{1/2}$/V			
compound	red	ox_1	ox_2	ΔE_g/eV[b]
Pt_2BTD-Th	−1.76	+0.30	+0.46	2.03
p-PtBTD-Th	−1.74	+0.29[c]	+0.73[c]	2.02
Pt_2BTD-EDOT	−1.89	+0.01	+0.25	1.89
p-PtBTD-EDOT	−1.85	+0.01[c]	+0.41[c]	1.84

[a] In CH_2Cl_2 with 0.1 M $TBAPF_6$ as the supporting electrolyte, scanned at 100 mV s^{-1}. Referenced to Fc/Fc^+ as an internal standard. [b] Electrochemical gap determined by taking the difference between the first oxidation potential and the reduction potential of the species. [c] E^0 determined by DPV.

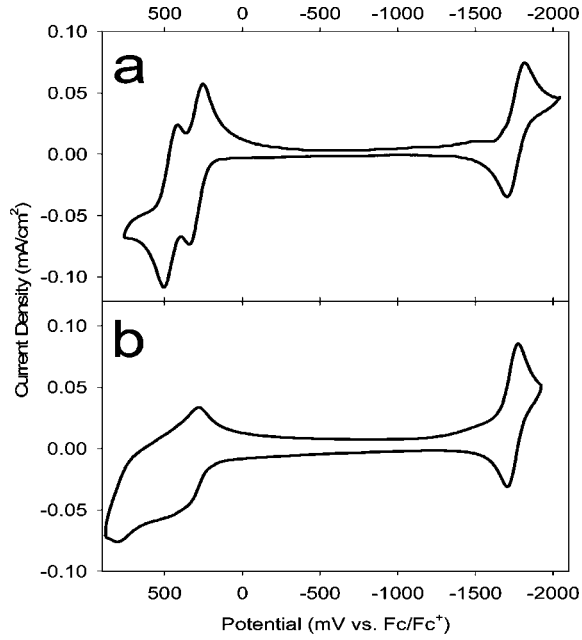

FIGURE 2. Cyclic voltammograms of (a) Pt_2BTD-Th and (b) *p*-PtBTD-Th in CH_2Cl_2 with 0.1 M $TBAPF_6$ as the supporting electrolyte, scanned at 100 mV s^{-1}. Potentials are referenced to Fc/Fc^+ as an internal standard.

BTD-EDOT (43, 44). (The reduction potentials for the free oligomers Th-BTD-Th and EDOT-BTD-EDOT are ca. $E_{1/2} = -1.55$ and -1.73 V, respectively, in V vs Fc/Fc^+) (45). Note that the reduction of the BTD-Th materials occurs at a potential approximately 100 mV less negative compared to that for the BTD-EDOT materials. This difference reflects the influence of the EDOT (donor) moieties, which slightly raises the energy of the lowest unoccupied molecular orbital (LUMO) level in the BTD-EDOT system relative to its position in the BTD-Th system.

As shown in Figure 2, the platinum acetylide oligomers and polymers also exhibit two oxidation waves that occur at potentials moderately anodic relative to Fc/Fc^+. The two waves are nicely reversible for the oligomers, whereas they are quasi-reversible for the polymers (compare the anodic branch of CVs in Figure 2). Like reductions, oxidations arise from electrophores concentrated on the π-conjugated organic segments. This assignment is supported by the fact that the first oxidation potentials for the oligomers and polymers correspond closely with the those of the corresponding free oligomers (43, 44). Importantly, the potential for the first oxidation waves for the BTD-Th materials are shifted positive by approximately 300 mV relative to those for the BTD-EDOT materials. This trend reflects the stronger donor nature of the EDOT moieties, which lead to a substantial increase in the energy of the highest occupied molecular orbital (HOMO) level in the BTD-EDOT materials.

The oxidation and reduction potentials of the oligomers and polymers were used to calculate the electrochemical HOMO−LUMO gap (E_g) of the materials, and the results are listed in the last column of Table 1. As expected, the BTD-EDOT materials exhibit a smaller E_g (~1.8 eV) compared to the BTD-Th materials (~2 eV). This difference reflects the strong donor property of the EDOT moieties, which raises the HOMO levels more than the LUMO levels, leading to a decrease in the band gap (relative to the BTD-Th materials). Note that there is only a small difference in E_g between the model compounds and the corresponding polymers. This result indicates that the HOMO and LUMO levels are concentrated on a single chromophore segment (e.g., Th-BTD-Th or EDOT-BTD-EDOT) rather than being delocalized over several repeat units. These E_g values agree closely with optical E_g values obtained by spectroscopic methods (vide infra). In addition to the electrochemical characterization of these compounds, reduction potentials of PCBM were measured in the same condition. The first and second reduction potentials were found to be -1.10 and -1.48 V, respectively.

Photophysical Characterization. The photophysical properties of the model compounds and polymers were characterized in a THF solution. The absorption and photoluminescence spectra of the materials are shown in Figure 3, and pertinent photophysical data are listed in Table 2. In general, all of the materials feature two primary absorption bands, one appearing in the near-UV or blue region of the visible and the second at lower energy with a maximum in the 550−650 nm region. Several features emerge upon close inspection of the absorption data. First, for each model

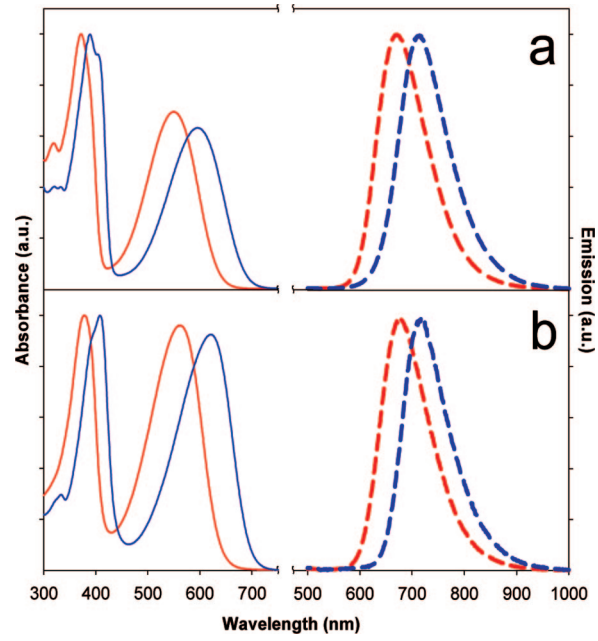

FIGURE 3. Absorption (solid line) and emission (dotted line) spectra of (a) Pt_2BTD-Th (red —, - - -) and Pt_2BTD-EDOT (blue —, - - -) and (b) *p*-PtBTD-Th (red —, - - -) and *p*-PtBTD-EDOT (blue —, - - -).

Table 2. Photophysical Properties of Model Compounds and Polymers[a]

compound	λ_{max}/nm	ε/cm^{-1} M^{-1}	λ_{em}/nm	Φ_f[b]	τ_f/ns	τ_{TA}/μs[c]	E_g/eV[d]
Pt_2BTD-Th	372	40 900	678	0.29	9.3	1.8	2.09
	549	28 400					
Pt_2BTD-EDOT	389	69 200	710	0.14	6.4	1.4	1.95
	596	43 800					
p-PtBTD-Th	378	45 600	683	0.04	1.1	1.1	2.07
	563	43 600					
p-PtBTD-EDOT	408	55 300	717	0.05	0.9	1.2	1.93
	621	51 100					

[a] In THF. [b] Excited at 510 nm, calculated using Rhodamine B ($\Phi_f = 0.69$) (47) in ethanol as an actinometer. [c] In ODCB. [d] Optical.

complex/polymer pair, the absorption band maxima are red-shifted for the polymers relative to the monomers. This feature suggests that there is some excited-state delocalization in the polymers relative to the monomers. This effect may arise via molecular orbital delocalization via dπ−pπ orbital overlap through the Pt centers (46). Alternatively, the red shift may result from exciton interactions between adjacent π-conjugated chromophores in the polymer systems. A second feature that is clear in the absorption spectra is that the band maxima for Pt_2BTD-EDOT and *p*-PtBTD-EDOT are red-shifted significantly compared to the band maxima for Pt_2BTD-Th and *p*-PtBTD-Th. This feature is consistent with the electrochemical band-gap calculations discussed above (Table 1) and results from the strong effect of the EDOT donor upon an increase in the HOMO level in the BTD-EDOT materials. The net result is that the presence of the strong EDOT donor lowers the band gap, resulting in a substantial red shift of both of the optical transitions.

All of the materials feature a broad, structureless (red) photoluminescence that is Stokes-shifted relatively little from the lowest energy absorption band. Quantum yields and

lifetimes of the emission are listed in Table 2. The photoluminescence decay lifetimes are in the range of a few nanoseconds, consistent with the assignment of photoluminescence to radiative decay from the singlet excited state (fluorescence). Despite the general similarity of the fluorescence from the materials, there are several significant differences that emerge from close inspection of the data. First, the trends noted for the absorption maxima are mirrored in the fluorescence spectra. Specifically, the fluorescence maxima are red-shifted in the polymers compared to the corresponding monomers, and the fluorescence maximum for the BTD-EDOT materials is red-shifted compared to the BTD-Th materials. The energy of the relaxed (fluorescent) singlet excited state (E_s) is estimated for each of the materials by using the onset wavelength for the fluorescence. The values are listed in Table 2, and they range from ~2.1 eV for the BTD-Th materials to ~1.95 eV for the BTD-EDOT materials.

The fluorescence quantum yields and lifetimes were determined for the materials in solution. The quantum yields are 3−5 times larger for the model complexes relative to the corresponding polymers. A similar trend is seen in the fluorescence lifetimes, which indicates that nonradiative decay is more efficient in the polymers. The more efficient nonradiative decay of the singlet state in the polymers likely arises from quenching sites (traps) in the polymers caused by interchain aggregation and possibly defects in the chain structure.

A key objective of this work is to explore the nature and photoactivity of the triplet states in the low-band-gap platinum acetylide materials. The observation of moderately efficient fluorescence and fluorescence (singlet) lifetimes in the nanosecond range suggests that intersystem crossing in the BTD-Th and BTD-EDOT materials is not as efficient as has been observed in platinum acetylide materials that have been previously investigated where singlet lifetimes <100 ps and triplet yields approaching unity have been reported (25, 48). Nevertheless, as outlined below, there is clear evidence that photoexcitation of all of the materials leads to at least a moderately efficient population of long-lived triplet states.

First, in efforts directed toward observing phosphorescence from the triplet states of the materials, a series of careful photoluminescence experiments was performed using a spectrometer equipped with a liquid-nitrogen-cooled InGaAs detector. Emission scans over the wavelength range 0.85−1.5 μm were carried out with the samples in solution (and solvent glass) at room temperature and at 80 K. Unfortunately, in all cases no detectable phosphorescence emission could be observed. This result is consistent with the previous report of Wong and co-workers, who also reported the absence of phosphorescence from *p*-PtBTD-Th in the near-infrared region (37).

Despite the inability to observe phosphorescence emission, clear evidence for the production of triplet states upon direct excitation of all of the materials was obtained by nanosecond to microsecond time-resolved absorption spectroscopy. Specifically, as shown in Figure 4, following 550 nm pulsed-laser excitation, degassed dichlorobenzene solutions of Pt_2BTD-Th and *p*-PtBTD-Th exhibit relatively strong transient absorption signals throughout the 350−800 nm region. The spectra are characterized by broad absorption over the entire visible region, peaking at ~700 nm, with negative (bleaching) bands that correspond to the ground-state absorption of the BTD-Th chromophore. For both materials, the transient gives rise to absorption decays with $\tau \sim 1-2$ μs, consistent with the assignment of the spectrum to the absorption of the triplet excited state. A close comparison of the spectra in Figure 4 shows that the transient absorption (ΔOD) is approximately 3 times larger for the model complex compared to the polymer. Given that the spectra were obtained on solutions having matched absorption (concentration) and the same laser power, this difference (although qualitative) suggests that the triplet yield is larger for the model complex compared to the polymer. Interestingly, this difference is consistent with the fluorescence yield and lifetimes, which indicate that the singlet state is quenched in the polymers. Apparently, singlet quenching in the polymers leads to a reduction in the triplet yield. Although the data are not shown, time-resolved absorption on the BTD-EDOT materials produced similar results; i.e., a triplet state is observed with a lifetime in the microsecond range and the transient absorption is stronger for Pt_2BTD-EDOT compared to *p*-PtBTD-EDOT, suggesting a higher triplet yield in the former.

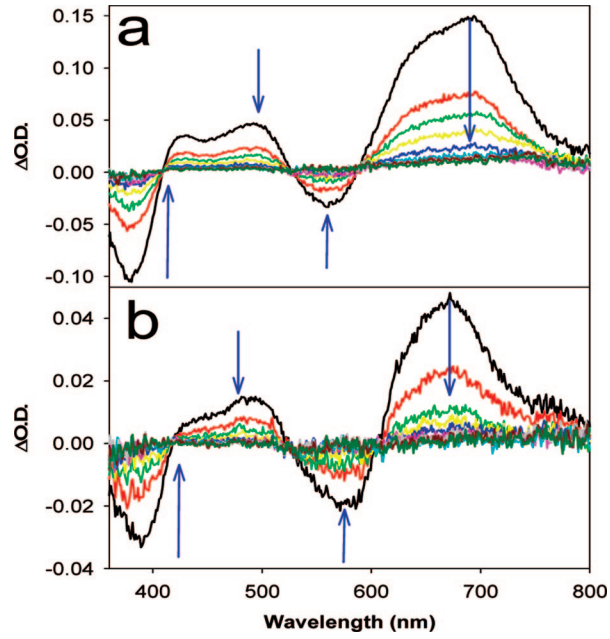

FIGURE 4. Transient absorption difference spectra of (a) Pt_2BTD-Th and (b) *p*-PtBTD-Th. Excited at 550 nm with 5 ns pulses. Spectra obtained with an initial 60 ns delay and with succeeding 1 μs delay increments. Arrows indicate the direction of change of spectra with increasing delay time.

PET and charge separation are key steps in the mechanism by which photovoltaic cells convert optical energy to electrical power (1, 4). As noted above, in a previous study, we confirmed that the triplet state of a platinum acetylide polymer was active in PET by demonstrating that PCBM

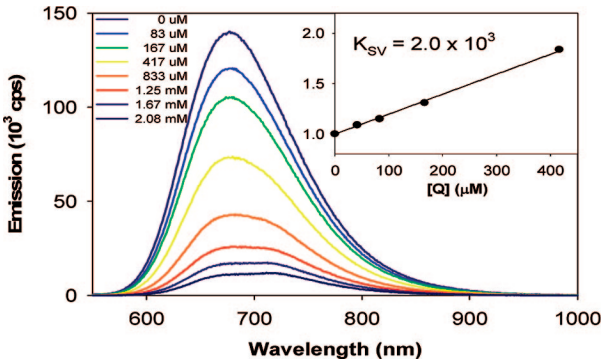

FIGURE 5. Fluorescence emission quenching of Pt_2BTD-Th by PCBM. The legend shows the concentration of PCBM in solutions, and the plot in the inset shows the Stern–Volmer plot of $I°/I$ vs [PCBM].

quenches the phosphorescence and, more importantly, by observing the products of PET by time-resolved absorption spectroscopy (15). Similar studies were conducted in the present investigation in order to probe the involvement of the triplet state in PET. Thus, transient absorption experiments were conducted with the platinum acetylide model complexes and the polymers in the presence of PCBM (c = 1 mM) in a dichlorobenzene solution. These experiments showed that in every case PCBM *does not* quench the triplet state and ion radicals resulting from charge separation were not observed. These results conclusively demonstrate that for the BTD-Th and BTD-EDOT materials the triplet is not involved in charge separation.

With that result in hand, we turned to experiments designed to probe whether PCBM interacts with the singlet state. For each of the materials tested, the addition of PCBM to dichlorobenzene solutions of the models (or polymers) was observed to quench the fluorescence efficiently. For example, Figure 5 shows the fluorescence spectrum of Pt_2BTD-Th in dichlorobenzene with PCBM added over the concentration range 0–2 mM. The inset illustrates the Stern–Volmer quenching plot, which is linear and affords a Stern–Volmer quenching constant $K_{SV} = 2.0 \times 10^3$ M^{-1}. Given the relatively short fluorescence lifetime, the large K_{SV} value suggests that static quenching may be the dominant quenching pathway. In parallel quenching experiments, it was observed that PCBM *does not* quench the lifetime of Pt_2BTD-Th, a result that confirms that static quenching occurs. Taken together, the fluorescence quenching results suggest that the addition of PCBM to Pt_2BTDTh results in the formation of a ground-state association complex (49, 50). Similar results were obtained when quenching experiments were carried out in Pt_2BTD-EDOT, indicating that in this case as well PET to PCBM only occurs from the singlet state and that a ground-state association complex is produced between the complex and PCBM in solution.

Optical Properties and Hole Mobility of Polymer Films. Because a focus of this project is on the performance of the organometallic polymers in bulk heterojunction solar cells, experiments were also carried out to characterize the optical and carrier mobility properties of the polymers as spin-coated films. For these experiments, neat polymer films were spin-cast on borosilicate glass and polymer/PCBM blend films were cast onto PEDOT-PSS-coated ITO substrates. First, careful experiments were carried out to determine the absorption coefficient of *p*-PtBTD-Th films. In these experiments, a series of four films of different thickness were fabricated and the absorption and reflectance spectra of the films were measured. Subsequently, the thickness of the same set of films was determined by atomic force microscopy (AFM). A thin film optical analysis was carried out as described in the Supporting Information, and this analysis provided estimates for the wavelength-dependent optical constants for the polymer (n and k; Figure S5a in the Supporting Information) as well as the absorption coefficient spectrum (Figure S5b in the Supporting Information). (The absorption coefficient spectrum is corrected for reflectance and is consistent across the set of four films.) The absorption spectrum of the *p*-PtBTD-Th film is similar to that of the material in solution. In particular, two primary bands are observed, with $\lambda_{max} = 383$ and 588 nm. Note that these bands are red-shifted somewhat from their positions in a THF solution (378 and 563 nm). The thin film optical analysis provides the absorption coefficients at 383 and 588 nm, and the values are $\alpha = 1.4 \times 10^5$ and 1.1×10^5 cm^{-1}, respectively. The absorption coefficient at 588 nm corresponds to a value of $\kappa = 0.51$ for the imaginary component of the refractive index. A similar set of thickness-dependent absorption experiments was carried out on a set of spin-coated films consisting of 4:1 (w/w) blends of PCBM and *p*-PtBTD-Th, and the results indicate that the absorption coefficient of the blend film is ~20% that of the pure polymer, with a value of $\alpha = 2.2 \times 10^4$ cm^{-1} at 576 nm. Using the α value for the blend film, we compute a value of $\kappa = 0.10 \pm 0.02$ at 576 nm. This is slightly lower than the κ value for a 4:1 blend of PCBM and *p*-PtBTD-Th reported by Wong and co-workers, which was determined by spectroscopic ellipsometry ($\kappa \approx 0.14$) (37).

In order to characterize the carrier mobility of films consisting of the organometallic polymers, hole mobilities were determined by space charge limited current measurements. In these measurements, a device configuration consisting of glass/ITO/PEDOT-PSS/polymer/Au was used, where the polymer is a spin-coated film of one of the organometallic polymers. In these measurements, the zero-field hole mobilities of *p*-PtBTD-Th and *p*-PtBTD-EDOT were determined to be $(1.4 \pm 0.3) \times 10^{-7}$ and $(1.1 \pm 0.2) \times 10^{-8}$ cm^2 V^{-1} s^{-1}, respectively. Note that the hole mobilities in both polymers are comparatively low [compared with poly(3-hexylthiophene), which has a mobility of ca. 10^{-3} cm^2 V^{-1} s^{-1}] (51) and also that the mobility of *p*-Pt-BTD-Th is an order of magnitude higher than that of *p*-PtBTD-EDOT (52, 53).

Photovoltaic Device Performance. The utility of the two polymers under study as light-absorbing and electron-donating materials to the electron acceptor PCBM for photovoltaic cells was investigated. Devices were constructed on PEDOT/PSS-coated ITO glass substrates by spin-coating blends from a toluene or *o*-dichlorobenzene solution. Each ITO substrate was masked and etched to allow an array of four active photovoltaic pixels having an area of 0.25 cm^2.

Table 3. *I*−*V* Characteristics of *p*-PtBTD-Th/PCBM Photovoltaic Devices[a]

solvent[b]	entry	thickness/ nm[c]	relative thickness[d]	V_{oc}/V	I_{sc}/mA cm^{-2}	FF	η/%
ODCB	K121	33	0.33	0.49	7.26	0.35	1.23
	K120	45	0.45	0.54	7.17	0.36	1.39
	K125	52	0.52	0.49	7.41	0.31	1.13
	K201	62	0.62	0.43	5.73	0.32	0.75
	K200	69	0.69	0.51	4.53	0.26	0.61
	K124	99	1.00	0.46	5.10	0.29	0.67
toluene	K185	38	0.50	0.51	4.42	0.33	0.65
	K184	50	0.66	0.59	6.49	0.34	1.28
	K190	68	0.89	0.54	5.70	0.29	0.9
	K233	76	1.00	0.40	4.01	0.31	0.51

[a] Average values of three pixels. [b] Used in spin-coating polymer/PCBM blends. [c] Photoactive layer. [d] Film thickness ratio relative to the thickest film in each set. Processing conditions: K120/K121, (300 rpm/1 min)/(300 rpm/2 min); K124/K125, (300 rpm/1 min)/(600 rpm/2 min); K200/K201, without/with 0.45 μm PTFE filter filtering; K184/K185, (500 rpm/2 min)/(1000 rpm/2 min); K190, 500 rpm/1 min and then 2000 rpm/1 min).

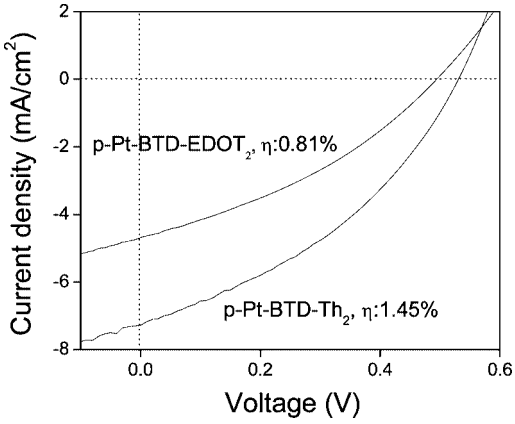

FIGURE 6. *I*−*V* characteristic curves of polymer/PCBM photovoltaic cells under AM1.5 simulated solar irradiation (100 mW cm^{-2}).

An aluminum electrode was then deposited onto the active layer by thermal evaporation under vacuum (note that a decreased performance was observed when a thin interlayer of LiF was employed). As noted in the results below, cell optimization required careful control of the spin rates and sample handling. Each entry reported in Table 3 is the average of at least three different pixels. Note that the entire process of active layer spin coating and electrode evaporation was carried out inside the inert-atmosphere glovebox, whereas the photovoltaic measurements were performed with the devices in air and without electrode encapsulation.

As demonstrated by the *I*−*V* characteristics of optimized pixels upon AM1.5 irradiation in Figure 6, it is evident that *p*-PtBTD-Th has an enhanced photovoltaic performance relative to *p*-PtBTD-EDOT. Examination of the data shows that this difference is mainly due to the increased short-circuit current (3−4 mA cm^{-2} for *p*-PtBTD-EDOT relative to ~7 mA cm^{-2} for *p*-PtBTD-Th). This is borne out in the spectral efficiency results of Figure 7, where *p*-PtBTD-Th shows a peak efficiency of 36% at 570 nm while *p*-PtBTD-EDOT shows a broadened response between 500 and 650 nm with an efficiency of ~ 15%. It is interesting that both

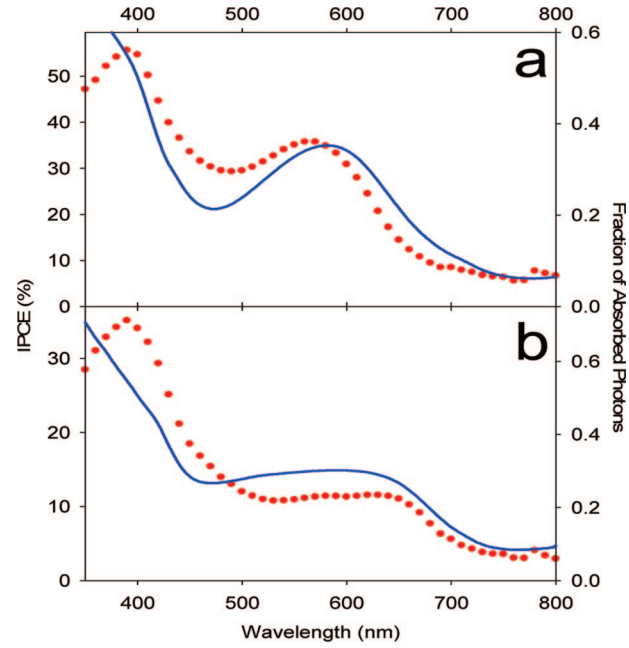

FIGURE 7. External quantum efficiencies (· · ·) and absorption spectra (—) of polymer/PCBM blend: (a) *p*-PtBTD-Th; (b) *p*-PtBTD-EDOT.

of these polymers demonstrate photovoltaic activity to wavelengths longer than 700 nm, as was designed using the donor−acceptor−donor triad for long-wavelength absorption. The distinct long-wavelength peaking of the absorption spectrum and IPCE response for *p*-PtBTD-Th relative to *p*-PtBTD-EDOT are likely due to the film quality and scattering from the *p*-PtBTD-EDOT/PCBM film in which aggregation was indicated in the GPC studies.

A close analysis of the results of Table 3 for the *p*-PtBTD-Th/PCBM devices indicates how important processing conditions and the film quality are with respect to the performance of the resulting photovoltaic devices. Films prepared from either ODCB or toluene could present similarly high AM1.5 efficiencies of 1.3−1.4%. In general, we (and others 8, 54, 55) find there is a "sweet spot" in the thickness of the photoactive materials in these devices. With films that are too thin, light absorption is reduced. More importantly, in the cells under study here, a dropoff in the I_{sc} is observed with an increase in the thickness. This is attributed to the relatively low hole mobilities exhibited by these polymers (vide supra). making charge collection difficult. Unfortunately, in our studies, we utilized a thin film profilometer for thickness measurements and found the absolute values to be somewhat inaccurate. (Ex-situ AFM thickness measurements suggest that the profilometer thickness values in Table 3 may be underestimated by a factor of ~2.) As such, the relative thicknesses showing a doubling or trebling in the set of cells studied in Table 3 are the best way to compare the results. While the cells' open-circuit voltages are relatively invariant, I_{sc} and the fill factors are distinctly affected. Overall, this work demonstrates that the *p*-PtBTD-Th/PCBM system has a strong photovoltaic activity; however, importantly in our hands, the response of these cells is not nearly as high as that reported previously (37).

Examination of the photovoltaic cell results for the *p*-PtBTD-EDOT/PCBM system (Table S1 in the Supporting Information) shows distinctly lower AM1.5 efficiencies ranging from 0.2 to 0.8%. These results are not nearly as consistent as the *p*-PtBTD-Th/PCBM cells and strongly point to the importance of the film quality due to the aggregation issues in this polymer. We do note that the power dependence of a *p*-PtBTD-EDOT/PCBM cell (Table S-2 and Figure S-4 in the Supporting Information) shows a linear increase in I_{sc} between 38 and 100 mW cm^{-2} with an invariant V_{oc}, as is expected for a properly functioning cell.

DISCUSSION

Mechanism and Energetics of Charge Separation in the Platinum Polymer/PCBM Blends. As noted in the Introduction, a key objective of this work is to probe for the involvement of the triplet excited state in organometallic photovoltaic materials. However, in order for the triplet excited state to be involved, the energetics for PET must be favorable. Thus, in this section, we consider the energetics of PET from the platinum polymers to PCBM for both the singlet and triplet excited states of the polymers.

The thermodynamic driving force for PET from the singlet or triplet state of a polymer to PCBM is given by the expression

$$\Delta G = E_{CS} - E_{es} \quad (1)$$

where E_{CS} is the energy of the charge-separated state and E_{es} is the energy of the singlet or triplet excited state (all states are referenced to the ground state of the polymer and PCBM) (16, 56, 57). The first term in this expression (E_{CS}) is given approximately by the difference in the oxidation potential of the donor (*p*-PtBTD-Th or *p*-PtBTD-EDOT) and the reduction potential of PCBM, i.e., $E_{CS} \approx E_{ox}$(polymer) − E_{red}(PCBM) (57, 58). By using the E_{ox} values for the polymers determined by electrochemistry (Table 1) combined with E_{red}(PCBM) = −1.10 V, the estimated E_{CS} values are 1.39 eV (*p*-PtBTD-Th/PCBM) and 1.11 eV (*p*-PtBTD-EDOT/PCBM). For the singlet excited states of the polymers, the second term in eq 1 can be determined from the onset of the fluorescence emission band, and these values are 2.07 eV (*p*-PtBTD-Th) and 1.93 eV (*p*-PtBTD-EDOT). Because the lack of phosphorescence emission precluded direct measurement of the polymers' triplet energies, the triplet energy levels are estimated by assuming a singlet−triplet splitting of 0.8 eV (22, 59, 60), affording values of ∼1.3 eV (*p*-PtBTD-Th) and ∼1.1 eV (*p*-PtBTD-EDOT). Using the estimated values for E_{CS} and E_{es} in eq 1, we can now see that for both polymers PET is exothermic from the singlet excited states (−0.57 and −0.63 eV for *p*-PtBTD-Th and *p*-PtBTD-EDOT, respectively), whereas PET is weakly endothermic from the triplet states (+0.1 and +0.05 eV for *p*-PtBTD-Th and *p*-PtBTD-EDOT, respectively).

The energetics for the *p*-PtBTD-Th/PCBM system are summarized in the Jablonski diagram provided in Scheme 3. This diagram makes it clear that the energy of the singlet state of the polymer is above that of the charge-separated state, and therefore PET is quite exothermic and, consequently, is anticipated to be rapid. By contrast, because the energy of the triplet state is slightly below that of the charge-separated state, PET from the triplet manifold is not expected to occur to any appreciable extent. (The Jablonski diagram for the *p*-PtBTD-EDOT/PCBM blend is similar and, therefore, is not shown.) The energetic considerations outlined here are in direct accord with the experimental observations. In particular, as outlined above, it was observed that in solution PCBM does not quench the transient absorption arising from the triplet state of either polymer. However, PCBM does efficiently quench the polymers' flurorescence, which indicates that PET from the singlet state is rapid. We conclude from this that in the active materials of the photovoltaic devices that were studied in this work only the singlet state is active in giving rise to charge carriers. Although the triplet excited state of the polymer does not contribute to charge separation, it could influence the efficiency of charge separation indirectly by providing a pathway for direct charge recombination to the lower-lying triplet state (61, 62).

Scheme 3. Energy Level Diagram for *p*-PtBTD-Th

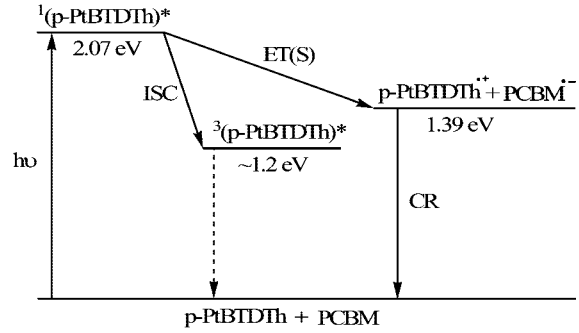

Table 4. Summary of *I*−*V* Characteristics of Polymer/PCBM OPVs[a]

compound	V_{oc}/V	I_{sc}/mA cm^{-2}	FF	η/%
p-PtTh [b]	0.64	0.99	0.43	0.27
p-PtBTD-Th	0.54	7.17	0.36	1.39
p-PtBTD-EDOT	0.50	4.56	0.35	0.78

[a] Illumination: AM1.5, 100 mW cm^{-2}. [b] Reference 15.

The performances of the photovoltaic devices based on *p*-PtBTD-Th or *p*-PtBTD-EDOT blended with PCBM are summarized in Table 4. Significant improvement in efficiency is observed for both devices in comparison to the efficiency of the *p*-PtTh/PCBM-based device we reported previously (15). The improvement in efficiency arises mainly because of a large increase (5−7-fold) in the short-circuit current density, which results from the considerably enhanced light absorption efficiency by the low-band-gap *p*-PtBTD-Th or *p*-PtBTD-EDOT materials. This result clearly demonstrates that the strategy to improve the photovoltaic performance via red shifting of the absorption profile of the active polymer was successful.

The second objective of this work was to harness the triplet exciton to generate charge in photovoltaic devices that are based on relatively low-band-gap polymers. However, on the basis of the thermodynamic analysis presented above and the solution triplet quenching data, it is evident that, even though the triplet state is produced with moderate

efficiency in both *p*-PtBTD-Th and *p*-PtBTD-EDOT, because of its low energy the triplet exciton is unable to undergo charge separation. This result points to a significant problem with the concept of harvesting the triplet exciton in photovoltaic devices. Specifically, for materials in which there is limited singlet−triplet mixing, the absorption spectrum is dominated by the spin-allowed transitions from the singlet ground state to the singlet excited state (63). As a result when considering charge separation from the triplet state, there is a significant loss of energy that occurs following photon absorption but before charge separation occurs. (The energy loss is analogous to a Stokes shift, but it includes losses due to both internal conversion within S_1 and intersystem crossing, $S_1 \rightarrow T_1$.) The amount of energy that is lost is approximately equivalent to the singlet−triplet splitting, which has shown to be a minimum of 0.7 eV in π-CPs (22, 59, 60). Thus, if the triplet state is to be active in charge generation, the material must have a sufficiently large band gap to overcome the energy loss associated with the singlet−triplet splitting (64). For a π-conjugated material with a HOMO level comparable to that of *p*-PtBTD-Th, the band gap must be above ca. 2.1 eV to ensure that the triplet exciton is sufficiently energetic to undergo charge separation. An alternative approach to solving this problem would be to use an organometallic material in which there is a much greater degree of singlet−triplet mixing (63). In this case, the direct singlet ground state to triplet excited state transition will be sufficiently allowed so that it contributes to the low-energy absorption of the material.

Comparison with Other Work. As noted in the Introduction, while the project described in the present paper was underway, a paper was published reporting that photovoltaic devices containing *p*-PtBTD-Th/PCBM blends as the active layer exhibit a peak IPCE of 87% at 580 nm and an overall AM1.5 power conversion efficiency in excess of 4.9% (37). While these results are significant and interesting, in the course of our work with the same active materials, we have been unable to attain comparably high photovoltaic device efficiencies. Specifically, as can be seen in Tables 3 and 4, careful optimization of processing conditions and the active layer thickness affords *p*-PtBTD-Th/PCBM-based devices that exhibit peak IPCEs of 36% and overall AM1.5 power conversion efficiencies of 1.39%.

Careful consideration of the available optical data suggests that the results reported herein for the *p*-PtBTD-Th/PCBM devices are in accordance with expectation given the intrinsic limitations of the active layer film thickness and light-harvesting efficiency. In particular, consideration of the absorption coefficient for the *p*-PtBTD-Th/PCBM blend films ($\alpha = 1.2 \times 10^4$ cm^{-1} for the 1:4 *p*-PtBTD-Th/PCBM blend) suggests that the active layer film thickness would need to be >200 nm in order for a device to operate with an IPCE of >85% at 580 nm (65). Although the measurements of the film thicknesses for the active layers in the photovoltaic devices reported herein are believed to underestimate the film thickness, the external quantum yields and power conversion efficiencies that we have measured are consistent with devices that operate with a high internal quantum efficiency but are limited in their overall performance because of incomplete light absorption by the active material. More specifically, the results are consistent with the expected performance of devices with active layers in the range of 75−125 nm that have high internal quantum efficiency but absorb only 30−40% of the incident light in the 550−600 nm region. While it may be coincidental, it is interesting to note that the performance reported herein for the *p*-PtBTD-Th/PCBM devices is in good agreement with the optical modeling results reported by Janssen and co-workers (39, 40). Furthermore, in a recent paper, Jen and co-workers report that an optimized device containing a 4:1 blend of *p*-PtBTD-Th/PCBM as the active layer exhibited an AM1.5 power conversion efficiency of 1.32% with a short-circuit current of 4.2 mA cm^{-2} (53). These values are in good agreement with the findings reported herein, supporting the suggestion that the performance of the *p*-PtBTD-Th/PCBM devices is limited by incomplete light absorption by the active layer and low mobility, which limits the efficiency of cells with a thicker active layer.

SUMMARY AND CONCLUSIONS

Two types of platinum acetylide polymers featuring low-band-gap donor−acceptor π-conjugated chromophores were synthesized and characterized by electrochemical and photophysical methods. The polymers were also used to construct organometallic photovoltaic devices when blended with PCBM as an acceptor and electron-transporting material. The photovoltaic devices based on the low-band-gap polymers display considerably improved performances compared to devices based on blends of a wide-band-gap (blue-absorbing) platinum acetylide polymer. The results suggest that charge separation in the photovoltaic materials occurs with a high internal quantum efficiency, but the overall photovoltaic performance is limited by incomplete light harvesting and low carrier mobility.

The photophysical studies of the polymers reveal that, although a triplet excited state is produced following light absorption, it is too low in energy to undergo PET with PCBM. Studies carried out in solution demonstrate that quenching of the singlet state of the polymers by PCBM is efficient, and this leads to the conclusion that the photovoltaic response of the solid materials arises because of charge separation from the singlet state of the polymer. The results point to the fact that, in order to harness the triplet excitons for charge separation in low-band-gap materials, it would be necessary to manipulate the energy levels of either the polymer or the acceptor. For example, decreasing the reduction potential of the acceptor by 0.1−0.2 eV would make charge separation with the triplet state of either *p*-PtBTD-Th or *p*-PtBTD-EDOT energetically favorable (66). Alternatively, lowering the oxidation potential of the platinum acetylide polymer without changing the band gap could accomplish the same goal.

Supporting Information Available: Detailed synthetic procedures and characterization data including NMR spectra

for compounds, thermochromism of p-PtBTD-EDOT, MALDI mass spectrum of p-PtBTD-EDOT, CVs for model compounds, film absorption data, and detailed data on the photovoltaic performance including light intensity and thickness dependence. This material is available free of charge via the Internet at http://pubs.acs.org.

REFERENCES AND NOTES

(1) Brabec, C. J.; Sariciftci, N. S.; Hummelen, J. C. *Adv. Funct. Mater.* **2001**, *11*, 15–26.
(2) Brabec, C. J. *Sol. Energy Mater. Sol. Cells* **2004**, *83*, 273–292.
(3) Scharber, M. C.; Wuhlbacher, D.; Koppe, M.; Denk, P.; Waldauf, C.; Heeger, A. J.; Brabec, C. L. *Adv. Mater.* **2006**, *18*, 789–794.
(4) Sariciftci, N. S.; Smilowitz, L.; Heeger, A. J.; Wudl, F. *Science* **1992**, *258*, 1474–1476.
(5) Brabec, C. J.; Zerza, G.; Cerullo, G.; De Silvestri, S.; Luzzati, S.; Hummelen, J. C.; Sariciftci, S. *Chem. Phys. Lett.* **2001**, *340*, 232–236.
(6) Thompson, B. C.; Frechet, J. M. J. *Angew. Chem., Int. Ed.* **2008**, *47*, 58–77.
(7) Reyes-Reyes, M.; Kim, K.; Carroll, D. L. *Appl. Phys. Lett.* **2005**, *87*, 083506.
(8) Li, G.; Shrotriya, V.; Huang, J. S.; Yao, Y.; Moriarty, T.; Emery, K.; Yang, Y. *Nat. Mater.* **2005**, *4*, 864–868.
(9) Kim, Y.; Cook, S.; Tuladhar, S. M.; Choulis, S. A.; Nelson, J.; Durrant, J. R.; Bradley, D. D. C.; Giles, M.; Mcculloch, I.; Ha, C. S.; Ree, M. *Nat. Mater.* **2006**, *5*, 197–203.
(10) Kim, J. Y.; Kim, S. H.; Lee, H. H.; Lee, K.; Ma, W. L.; Gong, X.; Heeger, A. J. *Adv. Mater.* **2006**, *18*, 572–576.
(11) Kim, K.; Liu, J.; Namboothiry, M. A. G.; Carroll, D. L. *Appl. Phys. Lett.* **2007**, *90*, 163511.
(12) Kim, J. Y.; Lee, K.; Coates, N. E.; Moses, D.; Nguyen, T. Q.; Dante, M.; Heeger, A. J. *Science* **2007**, *317*, 222–225.
(13) Green, M. A.; Emery, K.; Hishikawa, Y.; Warta, W. *Prog. Photovoltaics* **2008**, *16*, 61–67.
(14) Padinger, F.; Rittberger, R. S.; Sariciftci, N. S. *Adv. Funct. Mater.* **2003**, *13*, 85–88.
(15) Guo, F. Q.; Kim, Y. G.; Reynolds, J. R.; Schanze, K. S. *Chem. Commun.* **2006**, 1887–1889.
(16) Guo, F.; Ogawa, K.; Kim, Y.-G.; Danilov, E. O.; Castellano, F. N.; Reynolds, J. R.; Schanze, K. S. *Phys. Chem. Chem. Phys.* **2007**, *9*, 2724–2734.
(17) Shao, Y.; Yang, Y. *Adv. Mater.* **2005**, *17*, 2841–2844.
(18) Giebink, N. C.; Sun, Y.; Forrest, S. R. *Org. Electron.* **2006**, *7*, 375–386.
(19) Holten, D.; Gouterman, M.; Parson, W. W.; Windsor, M. W.; Rockley, M. G. *Photochem. Photobiol.* **1976**, *23*, 415–423.
(20) Balzani, V.; Carassiti, V. *Photochemistry of Coordination Compounds*; 1970.
(21) Beljonne, D.; Wittmann, H. F.; Kohler, A.; Graham, S.; Younus, M.; Lewis, J.; Raithby, P. R.; Khan, M. S.; Friend, R. H.; Bredas, J. L. *J. Chem. Phys.* **1996**, *105*, 3868–3877.
(22) Wilson, J. S.; Chawdhury, N.; Al-Mandhary, M. R. A.; Younus, M.; Khan, M. S.; Raithby, P. R.; Kohler, A.; Friend, R. H. *J. Am. Chem. Soc.* **2001**, *123*, 9412–9417.
(23) Kohler, A.; Wilson, J. S.; Friend, R. H.; Al-Suti, M. K.; Khan, M. S.; Gerhard, A.; Bassler, H. *J. Chem. Phys.* **2002**, *116*, 9457–9463.
(24) Silverman, E. E.; Cardolaccia, T.; Zhao, X. M.; Kim, K. Y.; Haskins-Glusac, K.; Schanze, K. S. *Coord. Chem. Rev.* **2005**, *249*, 1491–1500.
(25) Glusac, K.; Kose, M. E.; Jiang, H.; Schanze, K. S. *J. Phys. Chem. B* **2007**, *111*, 929–940.
(26) Wong, W. Y. *Dalton Trans.* **2007**, 4495–4510.
(27) Kohler, A.; Wittmann, H. F.; Friend, R. H.; Khan, M. S.; Lewis, J. *Synth. Met.* **1996**, *77*, 147–150.
(28) Zhang, Q. T.; Tour, J. M. *J. Am. Chem. Soc.* **1998**, *120*, 5355–5362.
(29) van Mullekom, H. A. M.; Vekemans, J. A. J. M.; Meijer, E. W. *Chem.—Eur. J.* **1998**, *4*, 1235–1243.
(30) Dhanabalan, A.; van Duren, J. K. J.; van Hal, P. A.; van Dongen, J. L. J.; Janssen, R. A. J. *Adv. Funct. Mater.* **2001**, *11*, 255–262.
(31) Thomas, C. A.; Zong, K. W.; Abboud, K. A.; Steel, P. J.; Reynolds, J. R. *J. Am. Chem. Soc.* **2004**, *126*, 16440–16450.
(32) Winder, C.; Sariciftci, N. S. *J. Mater. Chem.* **2004**, *14*, 1077–1086.
(33) Bundgaard, E.; Krebs, F. C. *Macromolecules* **2006**, *39*, 2823–2831.
(34) Steckler, T. T.; Abboud, K. A.; Craps, M.; Rinzler, A. G.; Reynolds, J. R. *Chem. Commun.* **2007**, 4904–4906.
(35) Blouin, N.; Michaud, A.; Leclerc, M. *Adv. Mater.* **2007**, *19*, 2295–2300.
(36) Blouin, N.; Michaud, A.; Gendron, D.; Wakim, S.; Blair, E.; Neagu-Plesu, R.; Belletete, M.; Durocher, G.; Tao, Y.; Leclerc, M. *J. Am. Chem. Soc.* **2008**, *130*, 732–742.
(37) Wong, W.-Y.; Wang, X.-Z.; He, Z.; Djurisic, A. B.; Yip, C.-T.; Cheung, K.-Y.; Wang, H.; Mak, C. S. K.; Chan, W.-K. *Nat. Mater.* **2007**, *6*, 521–527.
(38) Wong, W. Y.; Wang, X. Z.; He, Z.; Chan, K. K.; Djurisic, A. B.; Cheung, K. Y.; Yip, C. T.; Ng, A. M. C.; Xi, Y. Y.; Mak, C. S. K.; Chan, W. K. *J. Am. Chem. Soc.* **2007**, *129*, 14372–14380.
(39) Wong, W. Y.; Wang, X. Z.; He, Z.; Djurisic, A. B.; Yip, C. T.; Cheung, K. Y.; Wang, H.; Mak, C. S. K.; Chan, W. K. *Nat. Mater.* **2007**, *6*, 704–705.
(40) Gilot, J.; Wienk, M. M.; Janssen, R. A. J. *Nat. Mater.* **2007**, *6*, 704.
(41) Farley, R. T. Photophysics of Platinum and Iridium Organometallic Materials: From Molecular Wires to Nonlinear Optics. Ph.D. Thesis, University of Florida, Gainesville, FL, 2008.
(42) Wyatt, M. F.; Stein, B. K.; Brenton, A. G. *Anal. Chem.* **2006**, *78*, 199–206.
(43) Karikomi, M.; Kitamura, C.; Tanaka, S.; Yamashita, Y. *J. Am. Chem. Soc.* **1995**, *117*, 6791–6792.
(44) Blanchard, P.; Raimundo, J. M.; Roncali, J. *Synth. Met.* **2001**, *119*, 527–528.
(45) Corrected from vs SCE to vs Fc/Fc^{+}.
(46) Frapper, G.; Kertesz, M. *Inorg. Chem.* **1993**, *32*, 732–740.
(47) Parker, C. A.; Rees, W. T. *Analyst* **1960**, *85*, 587–600.
(48) Rogers, J. E.; Cooper, T. M.; Fleitz, P. A.; Glass, D. J.; McLean, D. G. *J. Phys. Chem. A* **2002**, *106*, 10108–10115.
(49) Datta, K.; Banerjee, M.; Seal, B. K.; Mukherjee, A. K. *J. Chem. Soc., Perkin Trans. 2* **2000**, 531–534.
(50) Bhattacharya, S.; Nayak, S. K.; Chattopadhyay, S.; Banerjee, M.; Mukherjee, A. K. *J. Phys. Chem. A* **2001**, *105*, 9865–9868.
(51) Bao, Z.; Dodabalapur, A.; Lovinger, A. J. *Appl. Phys. Lett.* **1996**, *69*, 4108–4110.
(52) While this paper was in revision, a report appeared in which the field-effect mobility of Pt-BTD-Th was measured to be 6.1×10^{-5} cm^2 V^{-1} s^{-1} with the material in a field-effect transistor configuration. See ref 53.
(53) Baek, N. S.; Hau, S. K.; Yip, H.-L.; Acton, O.; Chen, K.-S.; Jen, A. K. Y. *Chem. Mater.* **2008**, *20*, 5734–5736.
(54) Coakley, K. M.; McGehee, M. D. *Chem. Mater.* **2004**, *16*, 4533–4542.
(55) Valaski, R.; Canestraro, C. D.; Micaroni, L.; Mello, R. M. Q.; Roman, L. S. *Sol. Energy Mater. Sol. Cells* **2007**, *91*, 684–688.
(56) Oevering, H.; Paddonrow, M. N.; Heppener, M.; Oliver, A. M.; Cotsaris, E.; Verhoeven, J. W.; Hush, N. S. *J. Am. Chem. Soc.* **1987**, *109*, 3258–3269.
(57) Chen, P. Y.; Meyer, T. J. *Chem. Rev.* **1998**, *98*, 1439–1477.
(58) Here we are neglecting the correction term related to the difference in the solvation energy of the ion radicals in the solid film compared to the electrochemical solvent. See refs 56 and 57.
(59) Chawdhury, N.; Kohler, A.; Friend, R. H.; Wong, W. Y.; Lewis, J.; Younus, M.; Raithby, P. R.; Corcoran, T. C.; Al-Mandhary, M. R. A.; Khan, M. S. *J. Chem. Phys.* **1999**, *110*, 4963–4970.
(60) Wilson, J. S.; Kohler, A.; Friend, R. H.; Al-Suti, M. K.; Al-Mandhary, M. R. A.; Khan, M. S.; Raithby, P. R. *J. Chem. Phys.* **2000**, *113*, 7627–7634.
(61) Ohkita, H.; Cook, S.; Astuti, Y.; Duffy, W.; Heeney, M.; Tierney, S.; McCulloch, I.; Bradley, D. D. C.; Durrant, J. R. *Chem. Commun.* **2006**, 3939–3941.
(62) Ford, T. A.; Avilov, I.; Beljonne, D.; Greenham, N. C. *Phys. Rev. B* **2005**, *71*, 125212.
(63) Yersin, H. *Top. Curr. Chem.* **2004**, *241*, 1–26.
(64) Alternatively, an acceptor with a less negative reduction potential (lower LUMO) than PCBM must be used as the acceptor.
(65) Hoppe, H.; Arnold, N.; Sariciftci, N. S.; Meissner, D. *Sol. Energy Mater. Sol. Cells* **2003**, *80*, 105–113.
(66) Kooistra, F. B.; Knol, J.; Kastenberg, F.; Popescu, L. M.; Verhees, W. J. H.; Kroon, J. M.; Hummelen, J. C. *Org. Lett.* **2007**, *9*, 551–554.

AM800104K